IJMT. Vol. 21, Iss. 1, 2025. (12-27)

International Journal of Maritime Technology

Journal homepage: ijmt.ir

Hydrodynamic Performance and Stability Optimization of High-Speed Monohull Vessels with Chine Hulls: A Computational and Experimental Approach

Seyed Reza Samaei[1], Mohammad Asadian Ghahfarokhi[2*]

[1] Assistant professor, Technical and Engineering Faculty, Science and Research Branch, Islamic Azad University, Tehran, Iran; samaei@srbiau.ac.ir

[2] Assistant professor, Department of Marine industries, Science and Research Branch, Islamic Azad University, Tehran, Iran; m.asadian@srbiau.ac.ir*

ARTICLE INFO

Article History:
Received: 2 Feb 2025
Last modification: 22 Feb 2025
Accepted: 27 May 2025
Available online: 27 M ay 2025

Article type:
Research paper

Keywords:
high-speed vessel
hydrostatics
hydrodynamics
crew sea conditions
water ingress

ABSTRACT

High-speed monohull vessels with chine hulls are widely used due to their simple design, but maintaining optimal performance at high speeds requires precise hull force analysis. This study utilizes 3D scanning to capture hull geometry, refining it in AutoCAD for efficiency. Hydrostatic and hydrodynamic assessments are conducted using Maxsurf, applying the Switkowski method.

The study examines vessel motion, crew comfort, and water ingress under different sea conditions. Results indicate that at a 5.4-degree trim, pitch motion intensifies in harmonic waves, yaw motion increases in beam waves, and pitch and heave motions are more pronounced in head waves. Water ingress becomes a concern at this trim in Beaufort 2 and 3, with MSI peaking at 12.5% in Beaufort 3. The lowest resistance occurs at 5.22 knots, but higher trims raise power demands. Manual trim adjustments using outboard engines and jacks effectively mitigate these effects.

ISSN: 2645-8136

DOI: http://dx.doi.org/10.61882/ijmt.21.1.12

1. Introduction

Wave Interaction and Stability of Floating Structures

The interaction between waves and floating structures is a fundamental aspect of marine engineering, influencing both the stability and dynamic response of vessels. This study focuses on the effects of trim angles on the motion and stability of floating structures when exposed to varying wave conditions. By examining harmonic, beam, and head waves across sea states classified within the Beaufort scale (levels 1 to 3), the research provides valuable insights into vessel behavior across different maritime environments.

The results indicate that a trim angle of 5.4 degrees significantly influences pitch motion in harmonic wave conditions, increasing its amplitude by 33 to 48 percent when compared to a neutral trim position. At the same trim angle, overall motion responses exhibit an increase ranging from 11 to 39 percent. In beam waves, where the encounter angle is 90 degrees, yaw and roll motions become significantly amplified, showing an increase of up to 75 and 83 times, respectively. Similarly, under head waves (180-degree encounter angle), pitch motion experiences an increase of 40 to 58 percent, while heave motion intensifies by approximately 9 to 30 percent. As wave conditions become more severe, particularly under Beaufort 2 and 3, water ingress into the operational deck becomes a concern, underscoring the importance of maintaining vessel stability under challenging sea conditions.

Additionally, the study explores the interplay between trim angle and vessel speed. The findings suggest that achieving speeds beyond 60 knots requires a minimum trim angle of 5.4 degrees, although this comes at the cost of increased hydrodynamic resistance and power demand. The lowest resistance is observed at around 5.22 knots; however, higher initial trim angles contribute to greater hull resistance. To mitigate these effects, manual trim control mechanisms in outboard engines equipped with jacks prove to be essential.

These findings highlight the intricate role of trim angle adjustments in optimizing vessel motion, stability, and hydrodynamic performance. The insights provided in this study offer practical guidance for maritime engineers and designers in enhancing vessel operability under diverse sea conditions.

Hydrodynamic Aspects of High-Speed Boats

High-speed boats serve various functions, including law enforcement operations, emergency medical transport, and recreational activities [1]. Due to limitations in fuel capacity, provisions, and freshwater storage, these vessels are primarily used in nearshore environments, as they are not typically designed for long-distance travel in open waters [1]. Weighing between 2 and 10 tons, they generally achieve speeds in the range of 45 to 70 knots [2]. Compared to other high-speed watercraft, these vessels offer a cost-effective solution in terms of both production and maintenance [3].

To enhance speed and maneuverability, high-speed boats operate in planing mode, which minimizes hydrodynamic resistance [3]. Traditionally, these vessels featured long, narrow, round-bottomed hulls. Over time, however, their design evolved to incorporate transom sterns and V-shaped hulls, enabling them to reach Froude numbers exceeding 1.2 [4]. Various propulsion technologies, such as Direct Drive, Surface Drive, Stern Drive, and Vee Drive, have been developed to optimize vessel efficiency and operational performance [4].

The study of high-speed boat hydrodynamics has been a subject of extensive research over the years. Early work by Brown (1971) introduced investigations into planing surfaces equipped with trim flaps, while Savitsky and Brown (1975) contributed to the hydrodynamic evaluation of planing hulls [5][6]. With advancements in computational techniques, researchers such as Bizzolara (2003) and Molini & Brizzolara (2005) utilized Computational Fluid Dynamics (CFD) to study interceptor performance [7][8]. Complementing computational approaches, experimental studies—including Hansvic's (2005) research on stepped planing catamarans—have provided empirical validation of numerical models [9].

Ongoing research continues to focus on performance-enhancing technologies such as interceptors and stepped hulls [10]. Foundational principles, including Schlichting's (1979) boundary layer theory, offer critical insights into fluid flow behavior over planing surfaces [11]. More recent studies extend these findings to drag reduction strategies in high-performance marine vessels, further refining hydrodynamic efficiency [12].

These continuous advancements in vessel design emphasize the role of aerodynamics, structural optimization, and propulsion innovations in improving high-speed boat performance.

Geometric Modeling and Implementation Methodology

Developing an accurate geometric model of a vessel for construction is a detailed and resource-intensive

process. In this study, the hull lines were initially extracted using three-dimensional scanning techniques, followed by structural refinements to produce an optimized offset table. A preliminary shell model was generated using triangular flat surfaces, known as triangular meshes, to approximate the vessel's geometry. Although this method ensures a high degree of accuracy, it presents certain limitations in capturing intricate structural details such as spray rails and the transom. The generated shell serves as a basis for stability, resistance, and seakeeping calculations, allowing for an evaluation of hydrostatic properties under various heeled and trimmed conditions.

The modeling process involves converting the scanned three-dimensional hull data into hull lines using AutoCAD software. Following this step, refinements are applied to key structural elements, including the spray rails and transom, while ensuring smooth transitions and eliminating discontinuities. The finalized hull lines are then imported into Maxsurf software, where the hull structure is reconstructed and integrated using advanced modeling tools. The final high-speed boat model, featuring an optimized hull configuration, is subsequently prepared for comprehensive hydrostatic and hydrodynamic analysis.

Table 1. Initial Technical Specifications of the Sample High-Speed Boat

Row	Boat Characteristic	Value
1	Length (L)	69.8
2	Beam (B)	26.82
3	Height (H)	10.71
4	Draft (D)	4.0
5	Cruising Speed of the Float (v)	45
6	Total Volume (V)	933.10
7	Trim Angle of the Bow (Θ)	195.15
8	Trim Amount	41.3
9	Angle of Transom Heel with Vertical Axis (β)	6.12

Next, the study investigates the potential risk of water ingress into the float's navigational area and crew compartment under wave conditions classified within Beaufort scale levels 1 to 3. The hydrodynamic response of the float is modeled under these sea states, with the evaluation of seakeeping performance based on the maximum significant wave height. To ensure a comprehensive analysis, a wave spectrum with a narrow bandwidth and a defined modal period is used, derived from statistical wave data collected from the southern Persian Gulf. The study considers wave impact angles ranging from 0 to 180 degrees, increasing in 30-degree increments, corresponding to in-phase waves (0°), beam waves (90°), and head waves (180°).

Additionally, hydrodynamic forces acting on the float are calculated to assess resistance and the power required at varying speeds. Based on these computations, the necessary thrust power for different motion scenarios is determined. The initial technical specifications of the high-speed boat analyzed in this study are summarized in the following table.

3D Scanning and Optimization of Boat Hull Lines

For this study, the hull of the sample vessel was digitized using a three-dimensional scanner developed by SENSE, a U.S.-based manufacturer. The scanning process generated output files containing highly detailed mesh data, formatted in STL and OBJ. These formats are widely compatible with various 3D modeling software, including SOLIDWORKS, CATIA, 3DMAX, and RHINO, allowing for visualization, refinement, and modification of the hull geometry.

The scanning procedure was conducted in three key stages, each documented with corresponding images:

1. **Marking Reference Points:** Identifying and marking key points on the boat hull to enhance scanning accuracy.
2. **Segmented Scanning on Land:** Capturing individual sections of the hull, including the bow, bottom, transom, and sides, while the boat was on dry land.
3. **Longitudinal Scanning in Water:** Conducting a final scan along the boat's length while it was in water to complete the digital model.

This structured approach ensured a precise and comprehensive digital reconstruction of the hull, facilitating further analysis and optimization of its hydrodynamic properties.

Figure 1: Marking points on the boat hull and scanning different sections of the boat on dry land.

The figures show the boat scan results on dry land. Edge discrepancies are due to hull twisting during scanning, caused by the lack of longitudinal and transverse frames in the estimated mold.

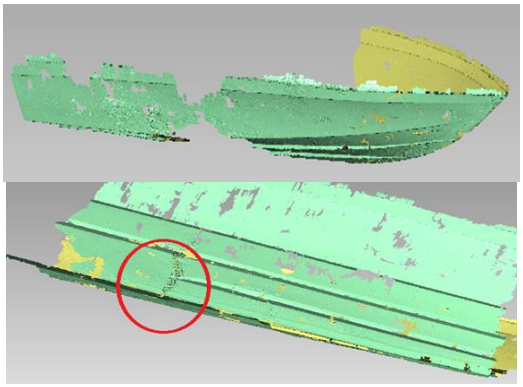

Figure 2: Results of scanning the sample boat and displaying differences in the edges.

To improve accuracy, certain boat sections were re-scanned. The refined results are shown in the figures below.

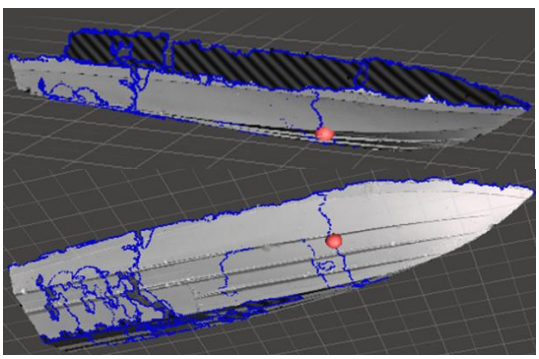

Figure 3: Re-scanning and presenting the final model of the boat on dry land.

The final model in Figure 3 required adjustments due to longitudinal distortion from lifting. To correct this, the boat was launched, aligned with measured dimensions, and re-scanned.

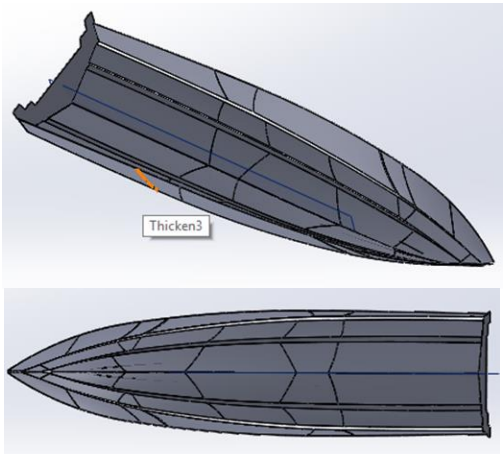

Figure 4: Accurate 3D scanning of the boat in water (final model).

Drawing Hull Lines and Offset Table

After 3D scanning the boat, a symmetrical and uniform geometry was generated. The raw hull data was converted into offset points using MAXSURF 20.00.01.59, which supports geometry modeling, equilibrium, resistance, and structural analysis.

For speedboat modeling, MAXSURF MODELER ADVANCED was used with NURB-based 3D surfaces. A sufficient number of offset points (markers) were entered to define the initial geometry. Unlike AutoCAD, where hull lines are primary outputs, in MAXSURF, they are derived from these surfaces.

To generate editable surfaces, cross-sections were approximated using markers (Figure 5). In AutoCAD, boat cross-sections were converted into continuous lines, followed by equal-interval point sampling. Since chines (spray strip edges) are critical in geometric modeling, the closest markers were precisely positioned to ensure accuracy.

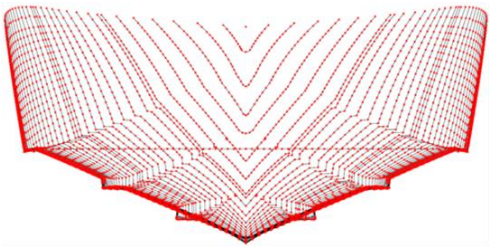

Figure 5: Display of float cross-sections and replacement offset points.

Final Scan Assumptions and Offset Point Adjustments

The final scanning process, along with adjustments to offset points (Figure 5), resulted in the establishment of several key assumptions:

1. **Measurement Reference Point:** The lowest point of the transom heel was selected as the measurement origin.
2. **Transom Heel as Baseline:** The transom heel was designated as section 0, serving as the reference for all subsequent measurements.
3. **Cross-Section Intervals:** Hull cross-sections were defined at intervals of 200 mm.
4. **Spray Strip Configuration:** The hull featured three pairs of water spray strips.
5. **Lowest Spray Strip Position:** The lowest spray strip extended from 2879 mm to 7141 mm along the hull.
6. **Waterline Design Reference:** The highest waterline angle at section 0 was measured at 40.0 meters from the baseline, establishing a key parameter in the boat's waterline design.
7. **Transom Heel Inclination:** The transom heel exhibited an inclination of 6.12° toward the heel.
8. **Bow Tip Location:** The bow tip was positioned 8534 mm from the transom heel.
9. **Keel Profile:** The keel maintained a straight profile from section 0 to 3200 mm before transitioning into a curved shape towards the bow.

These adjustments and assumptions provided a structured foundation for refining the hull's geometric model, ensuring accuracy in subsequent hydrodynamic and stability analyses.

Based on these parameters, the final hull lines were extracted, as shown in the following figures.

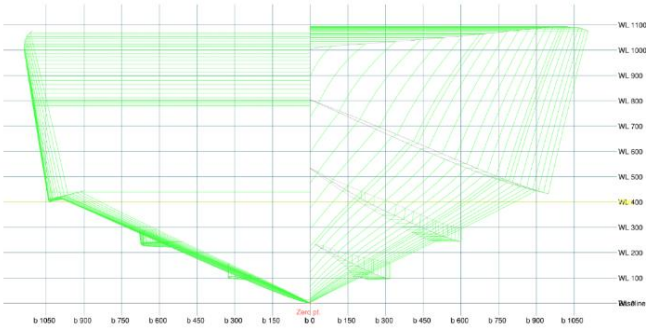

Figure 6: Display of transverse hull lines (sections of the left side heel and sections of the right-side chest).

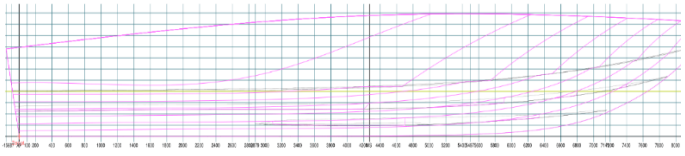

Figure 7: Display of longitudinal sections (with buttocks).

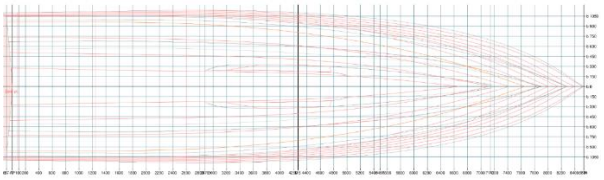

Figure 8: Display of float waterplanes.

Uniform Hull Generation for Hydrostatic and Hydrodynamic Calculations

To ensure a consistent hull for hydrostatic and hydrodynamic analysis, a uniform set of hydrodynamic lines was generated using corrected offset points and marker points along the hull. A fixed 3D coordinate system was established at the keel point in frame zero. Planes were then passed through each set of points. Since discontinuities occurred at connections, a 2.5 mm maximum deviation criterion was applied to ensure smooth and uniform planes. Points exceeding this deviation were adjusted to fit a new passing plane. For greater accuracy, side walls, spray rails, end plates, and bottom panels were modeled as separate planes, as shown in the following figures.

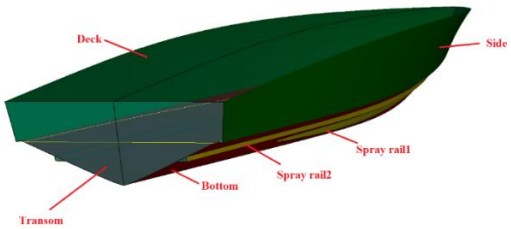

Figure 9: Definition of the main hull planes

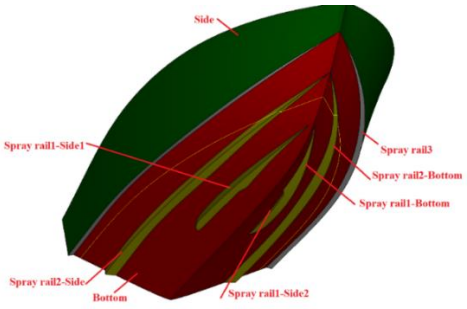

Figure 10: Definition and display of the spray rail planes

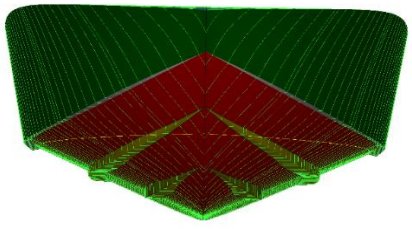

Figure 11: 3D visualization of the hull front view along with the transverse hull lines

Equilibrium, Resistance, and Seakeeping Calculations

Accurate final geometry modeling is essential for equilibrium, resistance, and seakeeping calculations of a high-speed boat. Fine triangular meshes in MAXSURF software are used, where the hull is represented by small triangular flat surfaces connecting adjacent markers. This mesh configuration (Figure 12) enables precise hydrostatic and hydrodynamic computations.

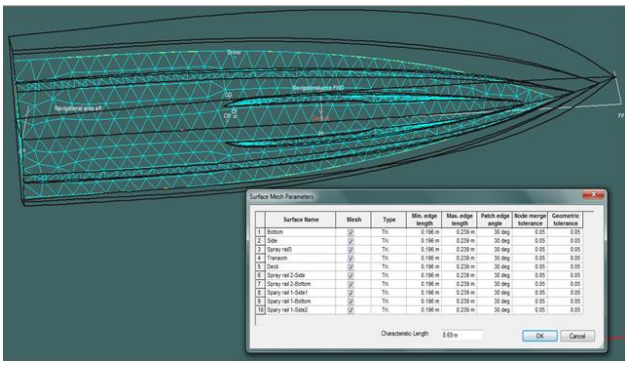

Figure 12: Modeling the hull bottom shell of the boat with triangular mesh in MAXSURF environment.

Coordinate System for Hydrostatic and Hydrodynamic Calculations

For accurate hydrostatic and hydrodynamic calculations, the following coordinate system is defined:

- Origin: Frame 0 at the lowest point of the transom heel (baseline).
- Longitudinal axis: Positive towards the bow.
- Vertical axis: Positive upwards.
- Transverse axis: Positive towards the right side, aligned with the hull's symmetry line.

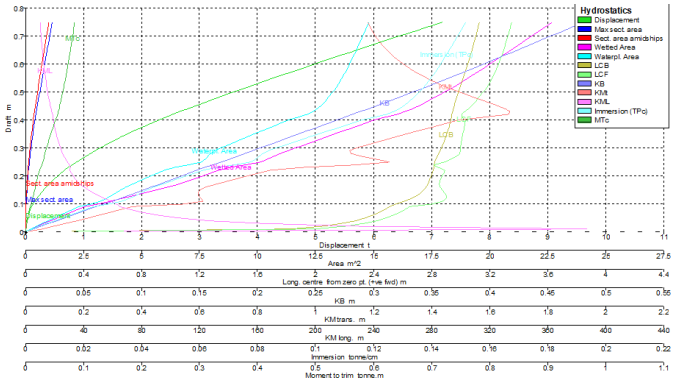

Figure 13: Curves of Variation in Important Hydrostatic Parameters at Different Waterlines for the Condition Without Heel and Trim

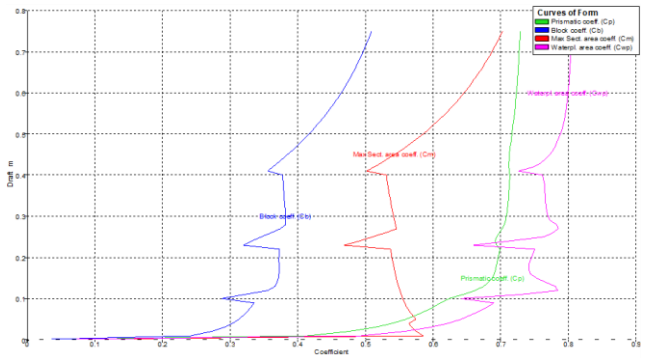

Figure 14: Curves of Variation in Hull Form Coefficients at Different Waterlines for the Condition Without Heel and Trim

Hydrostatic Calculations and Initial Trim Angle

Hydrostatic calculations are conducted without heel at various trim angles to achieve an optimal initial trim. Proper trim adjustment enhances cruising speed, reduces hull resistance, and minimizes slamming. However, trim adjustments are limited to ensure the vessel reaches planning while preventing excessive slamming or capsizing.

Hydrostatic parameters at different waterlines and trims (0 to 0.5 m in 0.1 m increments towards the stern) are detailed in Appendix 1. Given that a vessel's vertical center of gravity (KG) varies with loading and ballast, Cross Curves and KN curves are plotted for different conditions. For this high-speed boat, KG is set at 0.0 m, assuming all heel angles towards Starboard and a symmetric port side.

Figure 15 presents the results for zero-degree trim, with additional data available in Appendix 1.

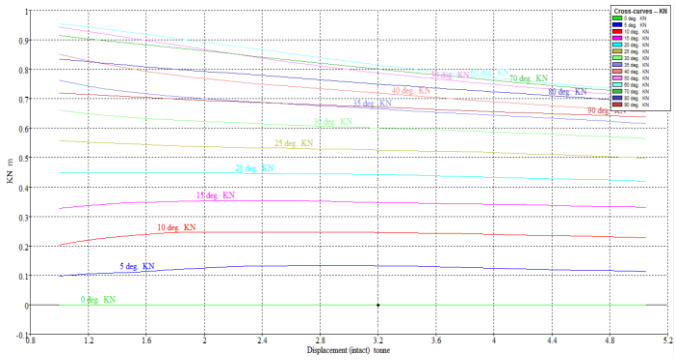

Figure 15: Cross Curves Curve at Zero Trim

Freeboard Length Calculation Results

Excessive water ingress is a primary cause of ship capsizing or sinking. Many vessels are designed to remain afloat even with multiple flooded compartments. However, ships may fail due to damage beyond design limits, inadequate pre-damage stability, or extreme weather conditions.

Given the smaller size of the high-speed boat in this study, flooding length calculations are critical for

assessing hydrostatic stability in a damaged state. The analysis is based on the following parameters:

- Initial trim: 0.0 m
- Vertical center of gravity (KG): 0.40 m
- Margin line distance to deck: 76 mm
- Displacement: 2.296 tons, average draft: 0.40 m
- Water penetration coefficient: 0.60 to 1.00 (in 10% increments)

The boat's general arrangement and compartment locations are illustrated in the following figure.

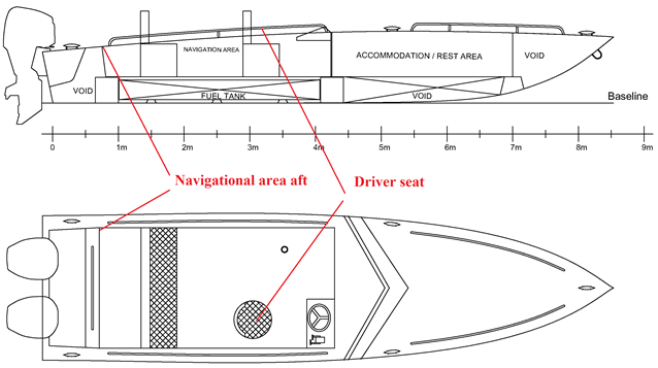

Figure 16: Initial Representation of Compartments and Spaces of the Boat

Purpose of Freeboard Length Calculations

The calculations aim to evaluate the boat's general layout compliance with freeboard length requirements. Specifically, the compartment lengths in the layout must not exceed the calculated flooding length, ensuring the boat maintains minimum stability even if a compartment becomes flooded.

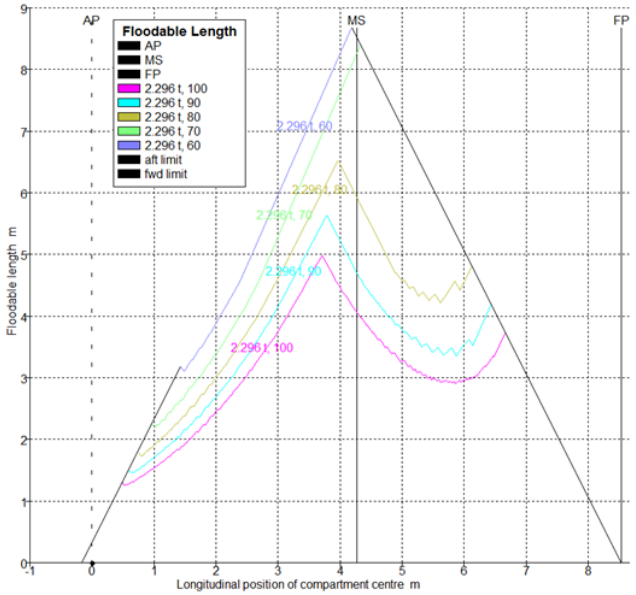

Figure 17: Length of Flooding vs. Different Penetration Coefficients

Referring to Figure 16, the boat is divided into four longitudinal regions from the stern to the bow. These four regions include the area behind the floatation area, the floatation area along with the fuel tank where occupants are present, the resting area and the empty space below it, and finally, the space in front of the collision bulkhead. In the table below, the lengths and centers of these spaces are listed and compared with the maximum flooding length obtained for different penetration coefficients (ranging from 60 to 100 percent with 10 percent increments).

Assumptions and Initial Conditions for Hydrostatic and Hydrodynamic Analysis

Before analyzing the ship's hydrodynamic behavior, key assumptions are considered to ensure a realistic evaluation:

- Water flow is non-rotational.
- Water is inviscid and incompressible.
- Deep water conditions are assumed.
- Linear potential theory is applicable due to small wave height and steepness.
- No forward speed is considered.
- Solution method: Linear potential theory & 3D Panel Method, based on radiation and diffraction theory using a boundary element method in the frequency domain. It provides Response Amplitude Operators (RAOs) but is limited to zero forward speed.
- Trim conditions: 0° and 5/4°, where 0° corresponds to the waterline trim, and 5/4° is optimal for resistance reduction.
- Ship geometry: Modeled with triangular panels (1634 panels for 0° trim, 1098 panels for 5/4° trim), with a maximum edge length of 24 cm.

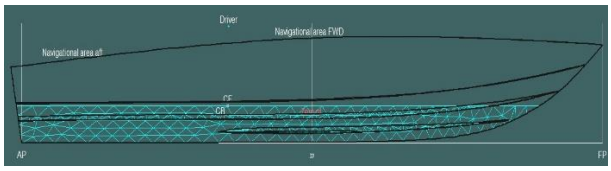

Figure 18: Float view at zero trim angle along with triangular panels used for wet surface modeling.

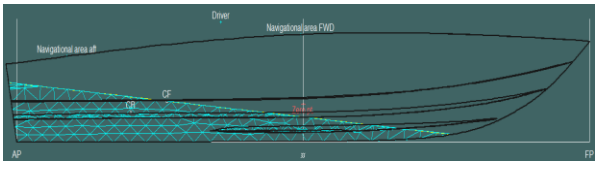

Figure 19: Float view at a 5/4-degree trim angle along with triangular panels used for wet surface modeling.

Additional Assumptions for Hydrostatic and Hydrodynamic Analysis

- Static heel angle: 0°.
- Roll motion results do not account for viscous damping.

- Gyroscopic radius assumptions:
  - Pitch & yaw motions: 25% of overall length.
  - Roll motion: 45% of overall beam.
- Center of gravity height: 0.629 m from the keel line, equivalent to the center of enclosed volume.

Environmental Wave Conditions

Hydrodynamic modeling considers Beaufort scales 1 to 3, using the maximum significant wave height to assess the boat's seaworthiness. The modal period is based on actual wave recordings from the South Pars region of the Persian Gulf, with a narrow-band spectrum applied. Wave incident angles range from 0° to 180° in 30° increments:

- 0°: Harmonious waves
- 90°: Beam waves
- 180°: Opposing waves

Range of Float Motions in Different Sea Conditions

The six-degree-of-freedom motions (surge, sway, heave, roll, pitch, yaw) were analyzed for Beaufort scales 1 to 3 at wave incident angles from 0° to 180° in 30° increments:

- 0°: Harmonious waves
- 90°: Beam waves
- 180°: Opposing waves

Results are presented in tables for each motion range under three statistical conditions:

- Mean Amplitude: Average motion range.
- Significant Amplitude: One-third larger than the largest motion ranges, representing practical external observation.
- Maximum Amplitude: Likely maximum motion over a long period, assuming constant Beaufort conditions.

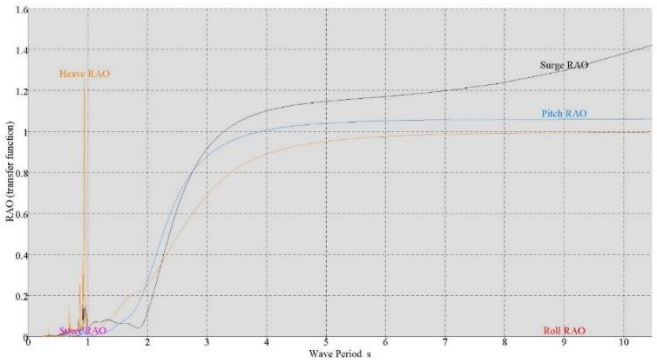

Figure 20: Float RAO for a static trim angle of 0 degrees at a wave incident angle of 0 degrees.

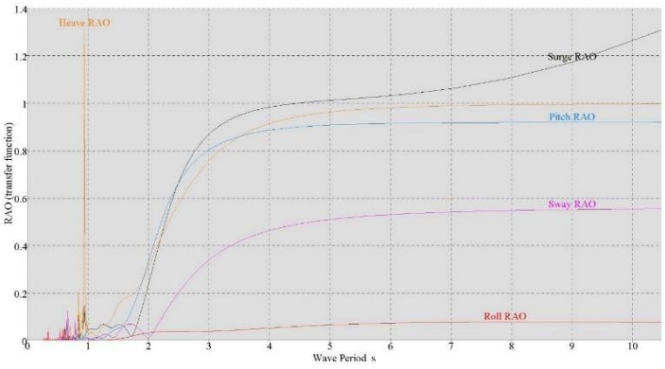

Figure 21: Float RAO for a static trim angle of 0 degrees at a wave incident angle of 30 degrees.

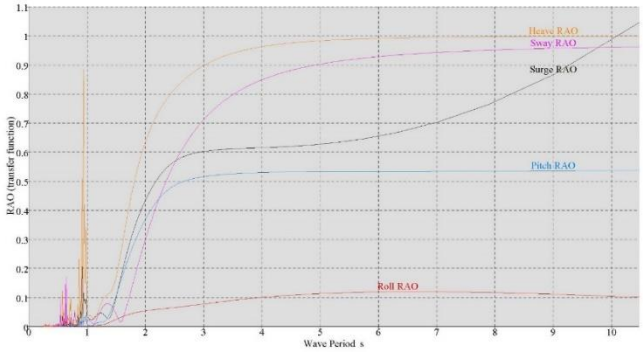

Figure 22: Float RAO for a static trim angle of 0 degrees at a wave incident angle of 60 degrees.

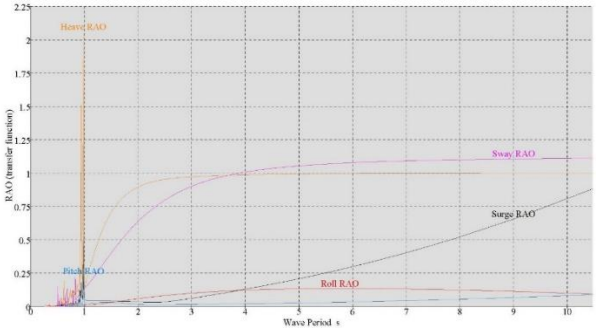

Figure 23: Float RAO for a static trim angle of 0 degrees at a wave incident angle of 90 degrees.

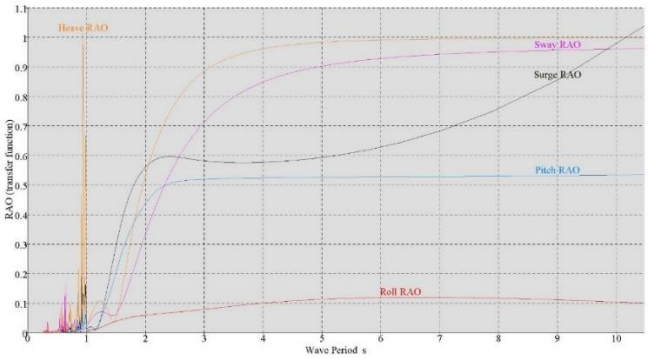

Figure 24: Float RAO for a static trim angle of 0 degrees at a wave incident angle of 120 degrees.

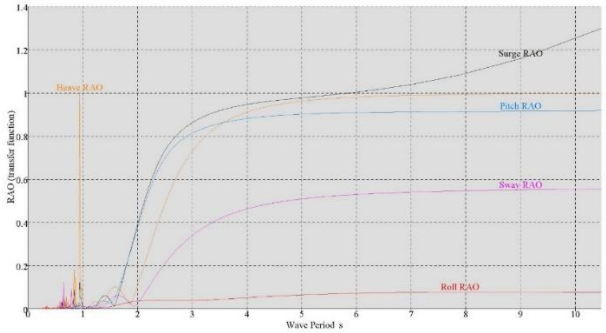

Figure 25: Float RAO for a static trim angle of 0 degrees at a wave incident angle of 150 degrees.

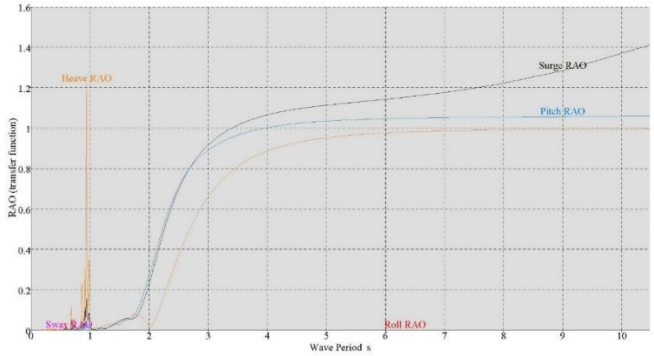

Figure 26: Float RAO for a static trim angle of 0 degrees at a wave incident angle of 180 degrees.

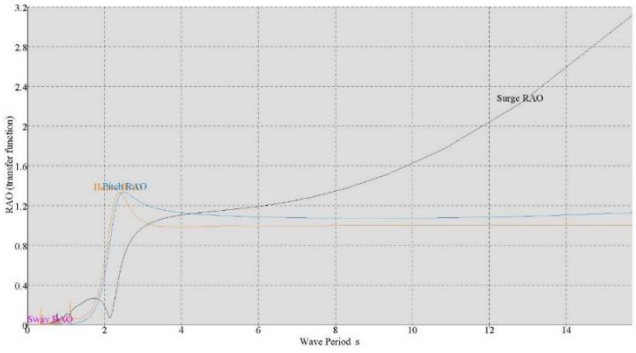

Figure 27: Float RAO for a static trim angle of 5/4 degrees at a wave incident angle of 0 degrees.

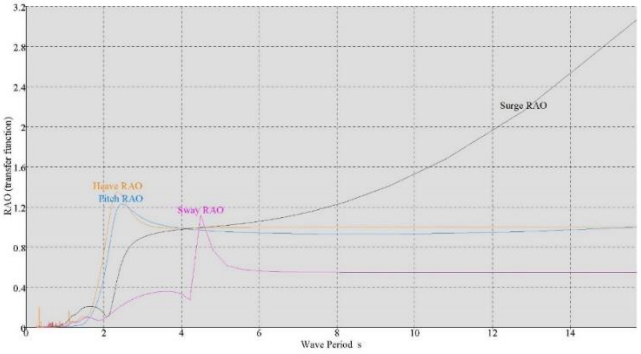

Figure 28: Float RAO for a static trim angle of 5/4 degrees at a wave incident angle of 30 degrees.

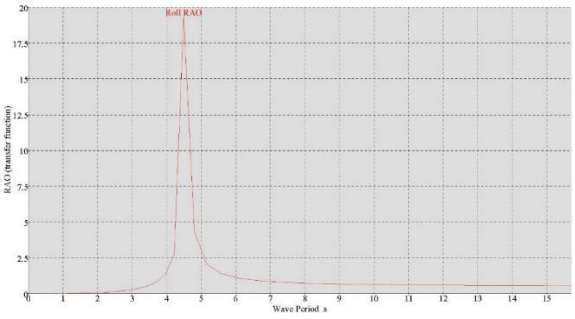

Figure 29: Float RAO for roll motion for a static trim angle of 5/4 degrees at a wave incident angle of 30 degrees.

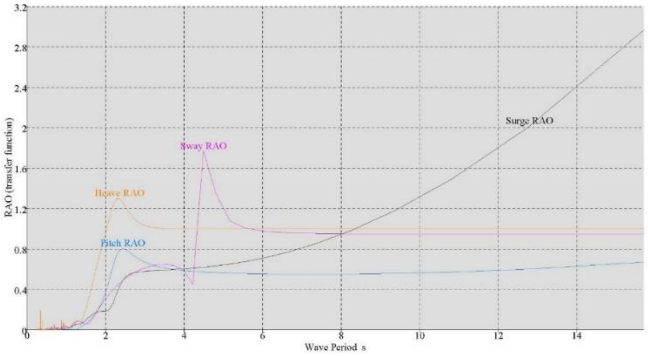

Figure 30: Float RAO for a static trim angle of 5/4 degrees at a wave incident angle of 60 degrees.

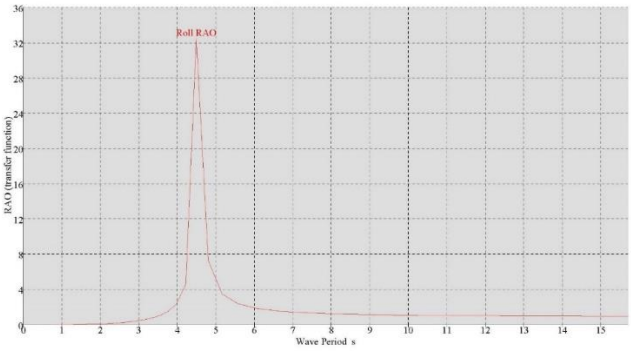

Figure 31: Float RAO for roll motion for a static trim angle of 5/4 degrees at a wave incident angle of 60 degrees.

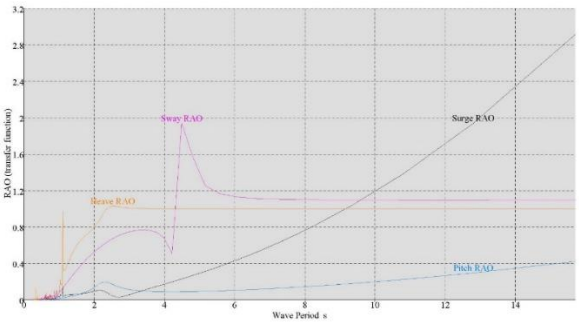

Figure 32: Float RAO for a static trim angle of 5/4 degrees at a wave incident angle of 90 degrees.

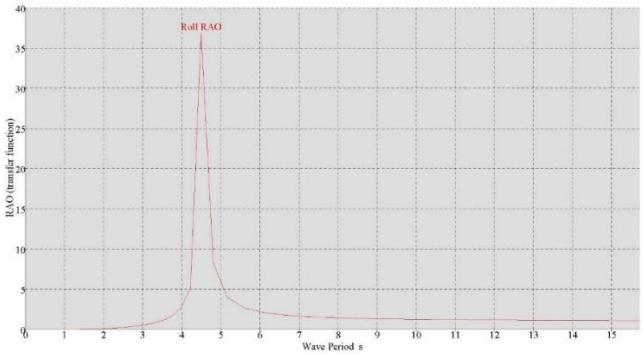

Figure 33: Float RAO for roll motion for a static trim angle of 5/4 degrees at a wave incident angle of 90 degrees.

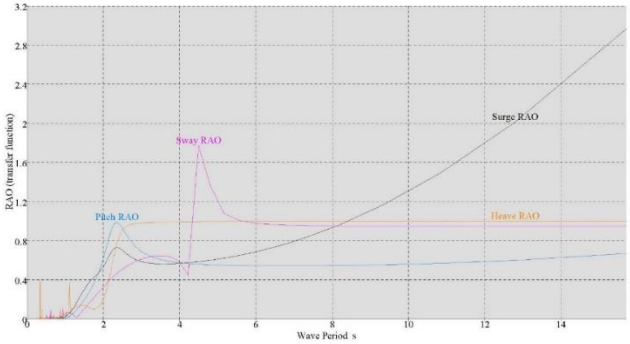

Figure 34: Float RAO for a static trim angle of 5/4 degrees at a wave incident angle of 120 degrees.

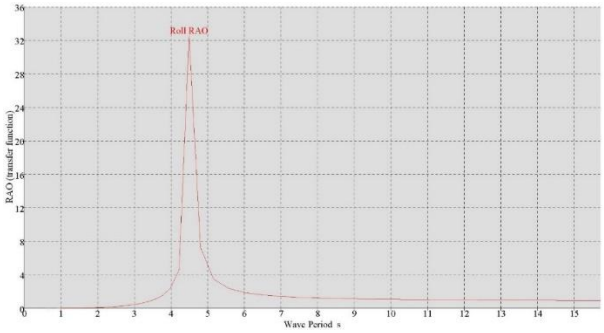

Figure 35: Float RAO for roll motion for a static trim angle of 5/4 degrees at a wave incident angle of 120 degrees.

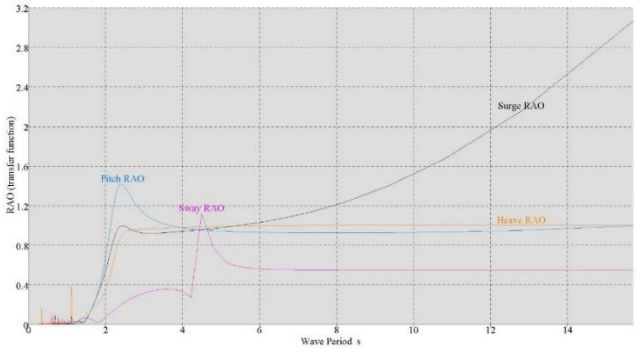

Figure 36: Float RAO for a static trim angle of 5/4 degrees at a wave incident angle of 150 degrees.

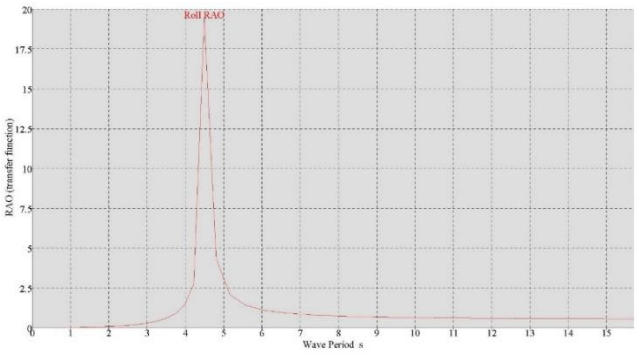

Figure 37: Float RAO for roll motion for a static trim angle of 5/4 degrees at a wave incident angle of 150 degrees.

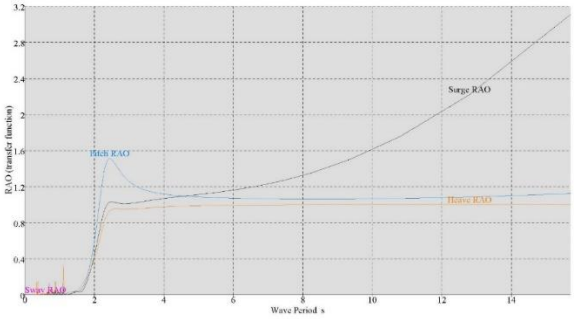

Figure 38: Float RAO for a static trim angle of 5/4 degrees at a wave incident angle of 180 degrees.

Water Ingress and Driver Seasickness Assessment

Probability of Water Ingress

The risk of water ingress into the navigational area aft was analyzed by comparing the relative vertical motion of the aft corners with the static freeboard:

- Static freeboard: 0.479 m (0° trim) and 0.333 m (4.5° trim).
- No ingress occurs at 0° trim for Beaufort 1 to 3.
- At 4.5° trim in beam waves:
    - Beaufort 2: 435 occurrences/hour
    - Beaufort 3: 617 occurrences/hour
    - This is highly undesirable as it leads to water entry.

Driver Seasickness Analysis

Two numerical metrics were evaluated:

1. MSI (Motion Sickness Incidence) – Measures the percentage of drivers experiencing nausea/vomiting due to vertical acceleration over 2 hours:
    - Beaufort 3 at 4.5° trim: 12.5% (~13 out of 100 drivers experience nausea).
    - Head-on & beam waves: MSI remains below 5%, indicating acceptable conditions.
2. SM (Subjective Magnitude) – Qualitative discomfort rating (0 to 30 scale):
    - 0 – 5: Moderate
    - 5 – 10: Serious
    - 10 – 15: Severe (Must "Hang On")

- 15 – 20: Hazardous
- 20 – 30: Intolerable

These results highlight the impact of trim angles and sea conditions on seakeeping performance and crew comfort.

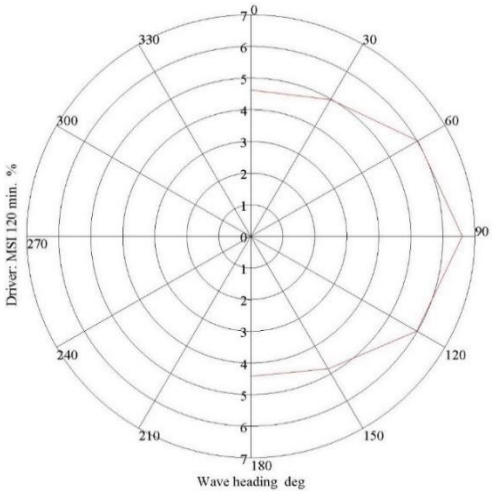

Figure 39: Polar Diagram of MSI Seasickness for a 2-hour Duration for the Driver's Seat at a Trim Angle of 0 Degrees and Beaufort 3.

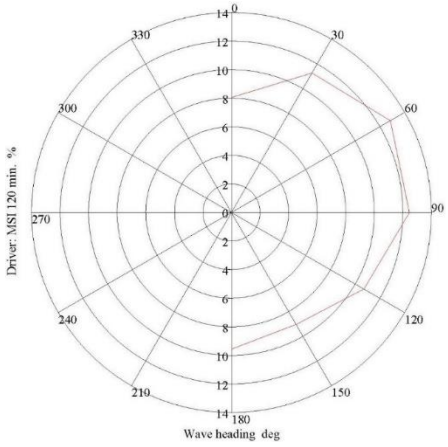

Figure 40: Polar Diagram of MSI Seasickness for a 2-hour Duration for the Driver's Seat at a Trim Angle of 5/4 Degrees and Beaufort 3.

Hydrodynamic Characteristics Calculation of the High-Speed Boat

Sewitsky's method, originally developed from resistance tests on various ship hulls, remains a key approach for estimating lift and drag forces on hydrofoil craft. Although later refinements have been introduced, it serves as the foundation for resistance calculations.

The total resistance (Rtotal) is composed of the following components:

- Pressure resistance (RPRESSURE)
- Frictional resistance (RFRICTION)
- Water spray resistance (RSPRAY)
- Air resistance (RAIR)
- Roughness resistance (RROUGHNESS) – added using the Townsin relationship (ITTC 2008) to account for surface roughness effects.

The frictional resistance coefficient is determined as follows:

- ITTC57 relationship for the turbulent region.
- Blasius relationship for Reynolds numbers (Rn) < 2×10^7.

The figure below illustrates the key parameters affecting the reference and upgraded Sewitsky methods used in these calculations.

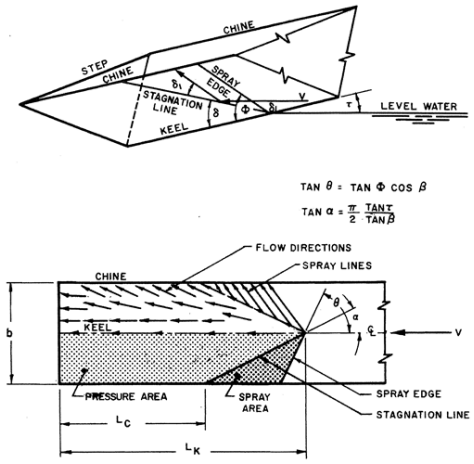

Figure 41: Representation of Key Parameters of the Reference and Upgraded Sewitsky Methods.

- Maximum beam: B
- Wetted length of the keel: LK
- Wetted length of the chine: LC
- Trim angle: τ
- Ratio of average wetted length to beam: λ
- Transverse flow number: FNB
- Chine bottom angle at mid-wetted length: β
- Longitudinal distance of the center of gravity from the transom heel: LCG

One of the fundamental assumptions of the Sewitsky method is that the hull of the vessel is at least partially hydrodynamic and that the chine angle remains constant along its length. The geometric inputs for the calculations in this study are outlined in the table below:

Table 1. Inputs for Hydrodynamic Resistance Calculations.

Row	Characteristic	Value	Description
1	Length of Waterline (LWL) (m)	681.7	For all LCGs at zero trim angle
2	Beam Width (B) (m)	0.832	The maximum beam width
3	Displaced Volume (m3)	19.2	Static displaced volume of the hull at zero speed
4	Projected Hull Area (m3)	962.3	Total projected hull area for air resistance calculation

Row	Characteristic	Value	Description
5	Air Drag Coefficient	0.70	According to the Svendsen suggestion for air resistance calculation
6	Bottom Inclination Angle (deg) β	7.23	Average bottom inclination angle at 5.0 meters aft (will yield the best results for high speeds)
7	Hull Average Roughness (µm) KS	150	Assigned to standard roughness for extending frictional resistance from model to float
8	Sea Water Density (kg/m3)	1026.021	Standard saline seawater density at 15 degrees Celsius
9	Air Density (kg/m3)	1.225	Air temperature at 15 degrees Celsius
10	Gravitational Acceleration (m/s2)	9.7915	Related to geographical latitude of 28 degrees suitable for the Persian Gulf

Optimization of Resistance and Effective Power

A key factor in optimizing resistance and effective power of a floating structure is selecting the longitudinal center of gravity and the initial static trim angle (θ_0).

Hydrodynamic calculations were conducted at various trim angles to:

- Identify the optimal propulsion system installation point.
- Determine the required effective power for speeds above 60 knots.

The analysis, based on hydrostatic data and hull resistance, was performed for:

- Initial static trim angle (θ_0).
- Optimal trim angle (6°).

The results are illustrated in the following figures.

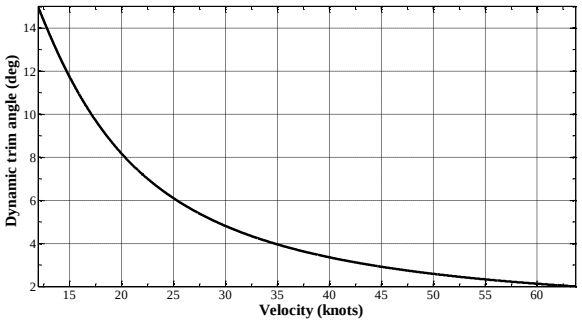

Figure 42: Dynamic trim angle of the floating structure at the initial trim angle of 6.0 degrees and LCG=1.483 m.

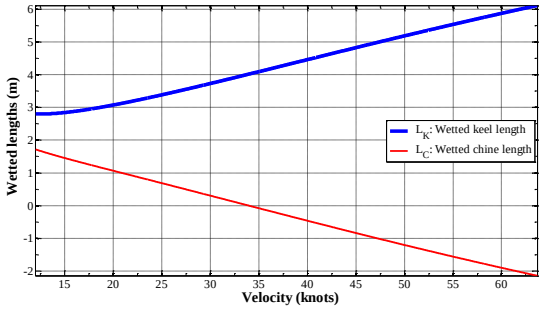

Figure 43: Length of keel line and wetted beam at the initial trim angle of 6.0 degrees and LCG=1.483 m.

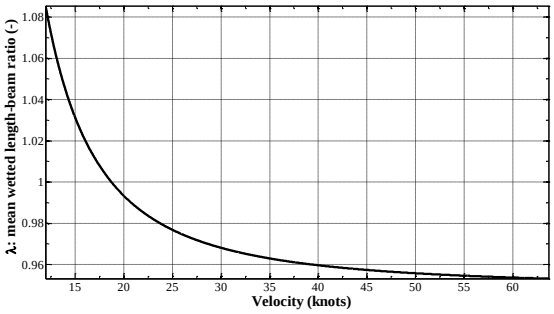

Figure 44: Ratio of average wetted length to beam width at the initial trim angle of 6.0 degrees and LCG=1.483 m.

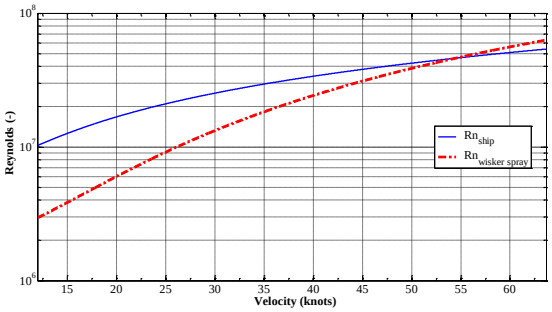

Figure 45: Reynolds number distribution and spray area at the initial trim angle of 6.0 degrees and LCG=1.483 m.

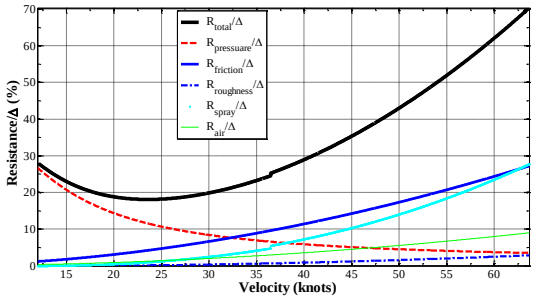

Figure 46: Ratio of resistance components to the weight of the floating structure at the initial trim angle of 6.0 degrees and LCG=1.483 m.

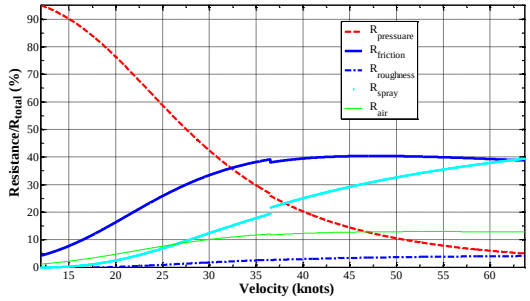

Figure 47: Analysis of the contribution of resistance components to total resistance at the initial trim angle of 6.0 degrees and LCG=1.483 m.

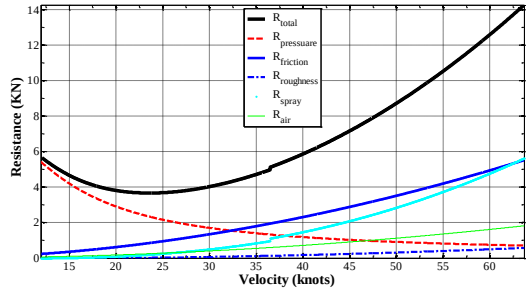

Figure 48: Evaluation of resistance of the floating structure at the initial trim angle of 6.0 degrees and LCG=1.483 m.

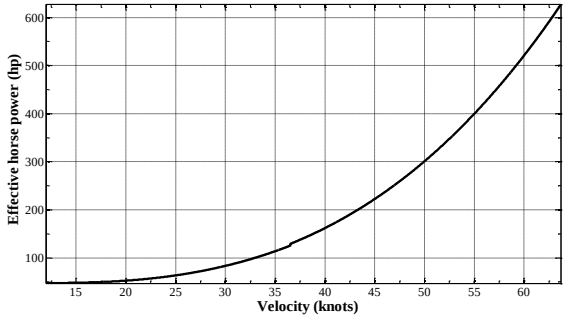

Figure 49: Examination of the required effective power of the floating structure at the initial trim angle of 6.0 degrees and LCG=1.483 m.

Academic Analysis of Trim Angle Effects on Floating Structures

This study examines the impact of trim angles on motion dynamics, water ingress, safety, speed, and resistance of floating structures under varying wave conditions. Key findings are summarized below:

1. Harmonic Waves (0° Encounter Angle)

- Pitch motion increases 33–48% at 5.4° trim compared to zero trim.
- Zero-degree encounter motion range rises 11–39% at 5.4° trim.

2. Beam Waves (90° Encounter Angle)

- Yaw motion increases 23–75 times at 5.4° trim.
- Roll motion increases 22–83 times, indicating significant instability.

3. Head Waves (180° Encounter Angle)

- Pitch motion range increases 40–58% at 5.4° trim.
- Heave motion rises 9–30%, affecting vertical stability.

4. Sea Conditions & Water Ingress Risk

- No water ingress at zero trim under Beaufort 1–3 conditions.
- At 5.4° trim, water ingress occurs in beam waves (Beaufort 2 & 3), which is undesirable for operational safety.

5. Maritime Safety Index (MSI) at Beaufort 3

- Maximum MSI: 12.5% at 5.4° trim, meaning ~13 out of 100 drivers may experience nausea in 2 hours.

6. Effect on Speed & Resistance

- Higher trim angles improve speed but increase resistance and required power.
- A minimum 5.4° trim is needed to exceed 60 knots.

7. Resistance at Specific Speeds

- Lowest resistance occurs at ~5.22 knots.
- Higher trim increases hull resistance at startup, requiring adjustments such as manual jack-equipped outboard engines.

This analysis highlights the trade-offs between trim angles, motion behavior, seaworthiness, safety, and efficiency in floating structures. Further experimental validation and computational modeling are necessary to refine optimal trim settings under various operational conditions.

Conclusion

The study provides valuable insights into the effects of trim angle on vessel motion, stability, and hydrodynamic performance under various wave conditions. Key findings are summarized as follows:

- **Harmonic Waves (0° Encounter Angle):** A trim angle of 5.4° leads to a significant increase in pitch motion, ranging from 33% to 48%, while the motion range at a zero-degree encounter angle rises

by 11% to 39% compared to a neutral trim condition.

- **Beam Waves (90° Encounter Angle):** Under beam waves, yaw motion intensifies by a factor of 23 to 75, and roll motion increases 22 to 83 times at a trim angle of 5.4°, highlighting substantial instability concerns.
- **Head Waves (180° Encounter Angle):** At the same trim angle, pitch motion increases by 40% to 58%, while heave motion rises between 9% and 30%, indicating notable dynamic responses in head wave conditions.
- **Risk of Water Ingress:** At zero trim, no water ingress occurs under Beaufort 1 to 3 conditions. However, at a 5.4° trim angle, water ingress becomes a concern, particularly in beam waves, occurring at a rate of 435 times per hour under Beaufort 2 conditions and increasing to 617 times per hour under Beaufort 3, which is undesirable for operational safety.
- **Maritime Safety Index (MSI):** The highest MSI value recorded was 12.5% at a trim angle of 5.4° under Beaufort 3 conditions, suggesting that approximately 13% of operators could experience motion sickness within a two-hour exposure period.
- **Speed and Resistance Relationship:** Increasing the trim angle facilitates higher speeds but also results in greater resistance and power demand. A minimum trim angle of 5.4° is required to surpass speeds of 60 knots.
- **Optimal Resistance Conditions:** The lowest resistance is observed at approximately 5.22 knots. However, higher initial trim angles contribute to increased hull resistance, particularly at startup, making floating ski conditions more difficult. To counteract this effect, outboard engines equipped with manual jacks allow for precise trim adjustments, helping to mitigate excessive resistance and optimize vessel performance.

These findings emphasize the complex relationship between trim angles, vessel dynamics, and operational efficiency. The study offers practical guidance for improving vessel stability, reducing risks, and optimizing hydrodynamic performance in varying maritime conditions.

8. References

1. Brown, P. W. (1971). An experimental and theoretical study of planning surfaces with trim flaps. Davidson Laboratory Technical Report.
2. Savitsky, D., & Brown, P. W. (1975). Procedures for hydrodynamic evaluation of planning hulls in smooth and rough water. In Proceedings of Hampton Road Section, SNAME (November 1975).
3. Dawson, D., & Blount, D. (2002). Trim control. Professional Boat Builder, N75.
4. Bizzolara, S. (2003). Hydrodynamic analysis of interceptors with CDF methods. In Proceedings Fast 2003, 7th Int. Conference on Fast Sea Transportation (Vol. 3, pp. E.49-E.56).
5. Molini, A., & Brizzolara, S. (2005). Hydrodynamics of interceptors: A fundamental study. In Proceeding ICMRT2005, Int Conference on Maritime Research and Transportation, Ischia (Naples), Italy (Vol. 1).
6. Villa, D., & Brizzolara, S. (2009). A systematic CFD analysis of flaps/interceptor's hydrodynamic performance. In Fast 2009, Athens, October 2009.
7. Steen, S., Alterskjar, S. A., Velgaard, A., & Aasheim, I. (2009). Performance of a planning craft with mid-mounted interceptor. In Fast 2009, Greece, October 2009.
8. Hansvic, T. (2005). Resistance of planning catamaran with step (MSc thesis). Department of Marine Technology, NTNU, Trondheim, Norway.
9. Hansvic, T., & Steen, S. (2006). Use of interceptors and stepped hull to improve performance of high-speed planning catamaran. In Int. Conf. on High-Speed Craft-ACV's Wig'd and Hydrofoils, Royal Institute of Naval Architecture, 31 Oct.-1 Nov., 2006, London, UK.
10. Fridman, G. (1969). Theory and practice of application of the interceptors on high-speed ships. In Fast 2007, Shanghai.
11. Chambliss, D. B., & Boyd, G. M., Jr. (1953). The planning characteristics of two V-shaped prismatic surfaces having angles of deadrise of 20° and 40°. NACA TN No.2876, January 1953.
12. Savirsky, D., & Neidlinger, J. W. (1954). Wetted area and center of pressure of planning surfaces at very low speed coefficients. Stevens Institute of Technology, Davidson Laboratory Report No.493, July 1954.
13. Savitsky, D., & Ross, E. (1952). Turbulence stimulation in the boundary layer of planning surfaces. Stevens Institute of Technology, Davidson Laboratory Report 44, August 1952.
14. Sottorf, W. (1932). Experiments with planning surfaces. NACA TM 661.
15. Locker, F. W. S., Jr. (1948). Tests of a flat bottom planning surface to determine the inception of planning. Navy Department, BuAer, Research Division Report No.1996, December 1948.
16. Sottorf, W. (1949). Systematic model researches on the stability limits of the DVI series of flow designs. NACA TM 1254, December 1949.
17. Davidson, K. S. M., & Locker, F. W. S., Jr. (1943). Some systematic model experiments on the

porpoising characteristics of flying boat hulls. NACA ARR, June 1943.

18. Benson, J. M. (1942). The effect of deadrise upon the low-angle type of porpoising. NACA ARR, October 1942.

19. Parkinson, J. B., & Olson, R. E. (1944). Tank tests of an army OA-9 amphibian. NACA ARR, December 1944.

20. Locker, F. W. S., Jr. (1943). General porpoising tests of flying-boat hull models. NACA ARR, September 1943.

21. Karafitah, G., & Fisher, S. C. (1987). The effect of stern wedges on ship powering performance. Naval Engineers Journal, May 1987.

22. Wang, C. T. (1980). Wedge effect on planning hulls. J. Hydronautics, Vol. 14, No. 4, 1980.

23. Cuasanelli, D. S., & Cave, W. L. (1993). Effect of stern flaps on powering performance of the FFG-7 class. Marine Technology, Vol. 30, No. 1, Jan. 1993.

24. Cuasanelli, D. S., & Karafiath, G. (2001). Advances in stern flap design and application. In Fast 2001, Southampton, UK, Sep. 2001.

25. Tsai, J. F., & Huang, J. K. (2003). Study on the effect of interceptor on high-speed craft. Journal of Society of Naval Architects and Marine Engineers, Roc, Vol. 22, No. 2, 2003, pp. 95-101.

26. Karimi, M. H. (2006). Hydrodynamic quality improvement techniques for high-speed planning crafts. In 7th Conference on Marine Industries, Tehran, Jan. 2006.

27. KSRI. (Year not provided). A radically new system for high-speed ship motion stabilization and speed increase based on automatically controlled interceptors, Report.2.

28. KSRI. (2004). A radically new system for high-speed ship motion stabilization and speed increase of oscillations of high-speed catamarans, Report.2004.

29. Karimi, M. H., Seif, M. S., & Abbaspoor, M. (2013). An experimental study of interceptor's effectiveness on hydrodynamic performance of high-speed planning crafts. Polish Maritime Research, 2(78), 2013, Vol. 20, pp. 21-29. DOI: 10.2478/pomr-2013-0013.

30. Schlichting, H. (1979). Boundary Layer Theory (7th ed.). McGraw-Hill Inc.

31. Interceptor Guide. (2011). Retrieved from http://www.humphree.com, March 15, 2011.

32. Day, A. H., & Cooper, C. (2011). An experimental study of interceptors for drag reduction on high-performance sailing yachts. Ocean Engineering, Vol. 38, pp. 983-994.

33. ITTC Recommended 2002 (for HSC model test).

34. Teimouri, M. (2009). The Effect of Spray Rails and Transverse Steps on High-Speed Vessels (Master's thesis).

35. Seyed Reza Samaei, Madjid Ghodsi Hassanabad, Mohammad Asadian ghahfarrokhi, Mohammad Javad Ketabdari, "Numerical and experimental investigation of damage in environmentally-sensitive civil structures using modal strain energy (case study: LPG wharf)". Int. J. Environ. Sci. Technol. 18, 1939–1952 (2021). https://doi.org/10.1007/s13762-021-03321-2

36. Samaei, S. R., Azarsina, F., & Ghahferokhi, M. A. (2016). Numerical simulation of floating pontoon breakwater with ANSYS AQWA software and validation of the results with laboratory data. Bulletin de la Société Royale des Sciences de Liège, 85, 1487-1499.

37. Samaei, S. R., Asadian Ghahferokhi, M., & Azarsinai, F. (2022). Experimental study of two types of simple and step floating pontoon breakwater in regular waves. International Journal of Marine Science and Environment, 6(1), 8-16.

38. Samaei, S. R., & Ghodsi Hassanabad, M. (2022). Damage location and intensity detection in tripod jacket substructure of wind turbine using improved modal strain energy and genetic algorithm. Journal of Structural and Construction Engineering, 9(4), 182-202. doi: 10.22065/jsce.2021.294103.2488

39. Samaei, S. R., Ghodsi Hassanabad, M., Asadian Ghahfarrokhi, M., & Ketabdari, M. J. (2021). Numerical and experimental study to identify the location and severity of damage at the pier using the improved modal strain energy method-Case study: Pars Asaluyeh LPG export pier. Journal of Structural and Construction Engineering, 8(Special Issue 3), 162-179. doi: 10.22065/jsce.2020.246425.2225

40. Samaei, S. R., Ghodsi Hassanabad, M., Asadian Ghahfarrokhi, M., & Ketabdari, M. J. (2020). Structural health monitoring of offshore structures using a modified modal strain energy method (Case study: four-leg jacket substructure of an offshore wind turbine). Journal Of Marine Engineering, 16(32), 119-130.

41. Samaei, S. R., Ghodsi Hassanabad, M., & Karimpor Zahraei, A. (2021). Identification of Location and Severity of Damages in the Offshore wind Turbine

Tripod Platform by Improved Modal Strain Energy Method. Analysis of Structure and Earthquake, 18(3), 51-62.

42. Samaei, S. R., Ghodsi Hassanabad, M., Asadian Ghahfarrokhi, M., & Ketabdari, M. J. (2021). Investigation of location and severity of damage in four-legged offshore wind turbine stencil infrastructure by improved modal strain energy method. Analysis of Structure and Earthquake, 17(3), 79-90.

43. Seyed Reza Samaei, Farhood Azarsina, Mohammad Asadian. " Numerical simulation of floating pontoon breakwater with Ansys Aqua software and validation of results with laboratory data.", The third national conference on recent innovations in civil engineering, architecture and urban planning, 2016.